PHYSICAL REVIEW B VOLUME 3, NUMBER 12 15 JUNE 1971

Sweepout and Dielectric Relaxation in Compensated Extrinsic Photoconductors*

A. Fenner Milton
Institute for Defense Analyses, Arlington, Virginia 22202

and

Morley M. Blouke
Texas Instruments, Incorporated, Dallas, Texas
(Received 16 November 1970)

Experimental evidence is presented concerning sweepout of majority carriers in p-type doped germanium photoconductors under high-resistivity conditions where the dielectric relaxation time τ_ρ exceeds the recombination time. This evidence demonstrates sweepout at signal modulation frequencies lower than the inverse dielectric relaxation time for the case of dc photoconductive gain greater than unity and gain saturation for signal modulation frequencies greater than the inverse dielectric relaxation time. These experimental findings are shown to be in general agreement with the predictions of a theoretical approach to semiconductor transport in this regime based upon the frequency dependence of the Debye length in compensated extrinsic photoconductors. This approach calculates the spatial dependence of the photoinduced hole concentration in the sample for an assumed boundary condition of $\Delta p = 0$ at the anode. This dependence is then used to predict an approximate maximum gain-bandwidth product in the form $GB \cong 1/\tau_\rho$. Lack of exact agreement between theoretical curves and experimental results can be explained by postulating an inhomogeneity in sample resistivity.

I. INTRODUCTION

Dielectric relaxation phenomena in p-type Hg-doped germanium photoconductors under high-resistivity cold-background conditions were first observed by Williams.[1] Dielectric relaxation appeared as a slow response time not associated with RC circuit effects or the recombination time of the material (τ). The appearance of a time constant on the order of the dielectric relaxation time τ_ρ (under conditions where $\tau_\rho \gg \tau$) was first associated with inhomogeneities in the material. However, further experiments showed that the falloff of response with increasing signal modulation frequency did not appear unless the dc photoconductive gain was greater than unity. For chopped signal illumination, the photoresponse was observed to saturate as the bias field was increased past the condition for unity dc photoconductive gain. On the basis of this observation, Williams associated the slow response with a majority-carrier sweepout phenomenon.[2] This general interpretation is still believed to be correct. In this paper, we will provide a microscopic model for the transport processes which are going on inside the photoconductive crystal and compare this model with more extensive experimental observations. The relevant calculations with the model are based on an assumed boundary condition $\Delta p = 0$ at the injecting anode.

Ryvkin has shown that for the case of steady signal illumination, the Debye length and effective drift length in extrinsic photoconductors are both extremely short for any reasonable degree of compensation and applied electric field.[3] Since the effective drift length is the range of influence of a discontinuity, an effective drift length shorter than sample dimensions means that the contacts cannot influence the carrier concentration in the bulk of the sample. This renders sweepout impossible. It has recently been shown, using the same sort of analysis as used by Ryvkin, that the Debye lengths in compensated extrinsic photoconductors are dependent on the signal modulation frequency. For chopped signal illumination, the effective drift length can become as long as the ordinary drift length[4] for modulation frequencies less than the inverse dielectric relaxation time, so that sweepout is possible for ac conditions.[5] It was proposed that this approach could be used to calculate the photoinduced hole distribution inside the sample and that if restrictive boundary conditions were applied at the contacts, sweepout would occur even for signal modulation frequencies less than the inverse dielectric relaxation time as long as the dc photoconductive gain was greater than unity.

It is the purpose of this paper to examine the consequences of the frequency dependence of the Debye length in detail and to compare sweepout predictions from this theory with detailed experimental observations on Hg-doped germanium samples which have dc photoconductive gains well in excess of unity.

II. THEORY

A. Material

An extremely simple energy-level model of a compensated p-type semiconductor can be used to describe an Sb-compensated Hg-doped germanium

extrinsic photoconductor at low temperatures. Infrared absorption and photoconductivity occur when electrons are excited from the valence band to the Hg acceptor impurity energy levels of density N_a at an energy ΔE above the valence band. Any shallower (unwanted) acceptor levels of density N_a' are considered to be already completely ionized by electrons coming from the compensator donor impurity (Sb) which has been added with density N_d. Since in a practical photoconductor $N_d > N_a'$, some of the infrared-active Hg-doped centers are ionized with density $n_0 = N_d - N_a'$ ($N_d \ll N_a$), even at $T = 0\,^\circ$K and cold backgrounds. The density n_0 can be controlled by varying the compensation density N_d.

We will be concerned here with lightly compensated Hg-doped germanium photoconductor material where $N_a = 10^{15}$–10^{16} cm^{-3} and $n_0 = 10^{12}$–10^{13} cm^{-3} measured at temperatures less than 27 °K with cold backgrounds. Under these experimental conditions the hole recombination time τ is controlled by the ionized acceptor density and is typically on the order of 10^{-6}–10^{-7} sec (i.e., $\tau \approx 1/\gamma n_0$, where γ is the recombination coefficient). The hole density and therefore the resistivity ρ and the dielectric relaxation time $\tau_\rho = \epsilon\rho/4\pi$ can be controlled by varying the effective infrared-background photon flux density J_b. At cold enough detector temperatures the hole density in the valence band p_0 can be approximated by $(J_b/t)\tau$ if the background radiation is completely absorbed (t is the sample thickness). For the cold backgrounds of interest, the resistivity is high ($p_0 \ll n_0$), leading to a τ_ρ greater than 10^{-3} sec. Table I provides a list of typical values for important parameters in the experimental situation of most interest.

B. General Solution

The approach which has been used to derive the frequency dependence of the Debye length assumed a one-dimensional continuous charge density model. Any possible trapping effects due to the compensated shallow acceptor states were neglected.

The hole density p at a given point in the sample can be changed either by drift or diffusion toward or away from that point, or by generation or recombination with ionized impurity centers at that point. The ionized impurity density n can vary with position, but at a given position this density can only be changed by generation or recombination since the impurities are immobile. The n_0 refers to the density of ionized impurities that would exist without the application of signal illumination, just as p_0 refers to the hole density that would exist without signal illumination.

TABLE I. Typical values for important experimental parameters.

T	27 °K
μ	2×10^4 cm^2/V sec
N_a	2×10^{15} cm^{-3}
N_d	4×10^{12} cm^{-3}
n_0	3×10^{12} cm^{-3}
τ	2×10^{-7} sec
t	0.5 cm
J_b	2×10^{10} cm^{-2} sec^{-1}
p_0	3×10^4 cm^{-3}
τ_ρ	10^{-2} sec
ΔE	0.086 eV

We will derive a general solution for the hole density p, analyze the case of partial signal illumination, discuss the most reasonable boundary conditions for the case of uniform signal illumination, and then calculate the effective gain of a photoconductor.

Although a portion of the available experimental evidence concerns the response to signal pulses, the case of sinusoidally modulated signal illumination will be considered here since the analysis is more straightforward. Maxwell's equations and the continuity equation can be used to derive the governing equation for the hole density in the sample. To get a realistic useful result, the conditions for charge neutrality need to be relaxed and a bipolar recombination rate r must be assumed ($r = \gamma np$). In the small-signal case, where the hole density induced by the infrared signal Δp is less than the hole density caused by the background flux and by the thermal generation rate p_0 (i.e., $\Delta p \ll p_0$), these equations can be linearized and combined to form

$$\frac{\partial^2 \Delta p_0}{\partial x^2} - \frac{eE_0}{kT}\frac{\partial \Delta p_0}{\partial x} - \frac{\Delta p_0}{[L_D(\omega)]^2} = F_{(\omega)} \tag{1}$$

and

$$\Delta n_0 = \frac{[\Delta g_0(N_a - n_0) - (\Delta p_0/\tau)](\tau_n)}{1 + i\omega\tau_n}, \tag{2}$$

where

$$L_D(\omega) = \left[\frac{e}{\mu kT}\left(\frac{1}{\tau_\rho} + i\omega\right)\left(1 + \frac{\tau_n}{\tau}\frac{1 - i\omega\tau_n}{1 + \omega^2\tau_n^2}\right)\right]^{-1/2} \tag{3}$$

and

$$F(\omega) = -\frac{\Delta g_0(N_a - n_0)\tau_n}{1 + i\omega\tau_n}\left(\frac{1}{\tau_\rho} + i\omega\right)\frac{e}{\mu kT} \tag{4}$$

for sinusoidal signal generation $\Delta g = \Delta g_0 e^{i\omega t}$.[5] Here $\Delta p = \Delta p_0 e^{i\omega t}$, $\Delta n = \Delta n_0 e^{i\omega t}$, $p = p_0 + \Delta p$, $n = n_0 + \Delta n$, k is Boltzmann's constant, T is the absolute temperature, e is the absolute magnitude of the electronic charge, E_0 is the applied electric field, μ is the hole mobility, $\tau_n = 1/(\gamma p_0)$ is the recombination time for the ionized impurity density under conditions where $\Delta p = 0$, $\Delta g(N_a - n)$ is the signal generation rate, and τ_ρ is the dielectric relaxation time, i.e., $\tau_\rho = \epsilon/(4\pi e\mu p_0)$ cgs, where ϵ is the low-frequency dielectric constant. $L_D(\omega)$ represents the frequency-dependent Debye length.

Since τ_n and τ_ρ both depend on the free hole density p_0, τ_n can be written as

$$\tau_n = \left(\frac{\partial r}{\partial n}\right)_{\Delta p=0} = \frac{1}{\gamma p_0} = \frac{1}{R^2}\,\tau_\rho\,, \tag{5}$$

where

$$R \equiv (\gamma\epsilon/4\pi e\mu)^{1/2} \tag{6}$$

is a basic parameter of the material (it does *not* depend on compensation level N_d or background flux J_b). Of course, μ is a function of N_a for neutral impurity scattering, and γ/μ or $(\mu\tau)^{-1}$ may have some temperature and electric field dependence, although this is usually not strong for temperatures above liquid-helium temperature. For the usual experimental situation the chopped infrared signal cannot be simply represented by $\Delta g_0 \cos\omega t$ as has been assumed so far, but must be represented by $\Delta g_0(1+\cos\omega t)$. However, since for the small-signal case the equations are linear, the principle of superposition applies and solutions for different frequencies can be considered to be additive, which allows the ac component to be considered separately without loss of physical content.

Equation (1) is a general equation for the small-signal case. However, in the discussions which follow we will be primarily concerned with the cold-background case where $\tau_\rho \gg \tau$. Since for the material of interest R is less than unity, τ_n, which represents the response time of the ionized impurities under conditions where $\Delta p = 0$, is usually the longest response time of the system. Estimates for R in Cu- and Hg-doped germanium with $T \leq 27\,^\circ$K and $N_a = 10^{15}$–10^{16} cm^{-3} vary between 0.1 and 0.01. The $R = 0.03$ has been chosen for all calculations presented here. This corresponds to $\mu \cong 2\times10^4$ cm^2/V sec and a captured cross section of $\langle\sigma\rangle = 10^{-11}$–$10^{-13}$ cm^2 with a thermal velocity of $v_{th} \cong 5\times10^6$ cm/sec ($\gamma \equiv \langle\sigma\rangle v_{th}$).[6,7]

Equation (1) can be solved for Δp_0

$$\Delta p_0 = \frac{\Delta g_0(N_a - n_0)\tau}{1 + (\tau/\tau_n) + i\omega t}\,(1 + Ae^{x/L_1} + Be^{x/L_2})\,, \tag{7}$$

where

$$\frac{1}{L_{1,2}} = \frac{eE_0}{2kT} \pm \left[\left(\frac{eE_0}{2kT}\right)^2 + \left(\frac{1}{L_D(\omega)}\right)^2\right]^{1/2}. \tag{8}$$

This is a general solution valid for both high and low backgrounds. The constants A and B must be determined by the boundary conditions. For small applied bias,

$$E_0 \ll |2kT/eL_D(\omega)| \tag{9}$$

diffusion dominates and

$$\frac{1}{L_{1,2}} = \frac{eE_0}{2kT} \pm \frac{1}{L_D(\omega)}\,, \tag{10}$$

but for the case of most interest,

$$E_0 \gg |2kT/eL_D(\omega)| \tag{11}$$

drift dominates, diffusion can be neglected, and

$$\frac{1}{L_1} = \frac{eE_0}{kT} + \frac{1}{L_{eff}} + \frac{i}{L'}\,, \tag{12}$$

$$\frac{1}{L_2} = -\frac{1}{L_{eff}} - \frac{i}{L'}\,, \tag{13}$$

where

$$L_{eff} = E_0\mu\tau\left(\frac{\tau}{\tau_\rho} + \frac{1/R^2}{1+\omega^2\tau_n^2} + \frac{\omega^2\tau_n^2}{1+\omega^2\tau_n^2}\right)^{-1} \tag{14}$$

and

$$L' = E_0\mu\tau\left[\omega\left(\tau + \frac{\tau_n}{1+\omega^2\tau_n^2} - \frac{\tau_n/R^2}{1+\omega^2\tau_n^2}\right)\right]^{-1}. \tag{15}$$

Figures 1 and 2 show the dependence of L_{eff} and L' on frequency. The solid line corresponds to a low-background case with $\tau_\rho/\tau = 10^4$ and the dashed curve corresponds to one particular high-background case, i.e., $\tau_\rho/\tau = 0.2$. As long as $\tau_\rho \gg \tau$, the low-frequency behavior can be scaled in terms of τ_ρ and $R\,\tau_\rho$ and is therefore insensitive to the particular value of τ_ρ/τ.

For $\omega = 0$,

$$L_{eff} = E_0\mu\tau(\tau/\tau_\rho + 1/R^2)^{-1} \sim E_0\mu\tau R^2, \tag{16}$$

when $\tau_\rho > R^2\tau$.

This is Ryvkin's result for the dc effective drift length.[3] Since R^2 is approximately 10^{-3} in Hg-doped germanium, for dc signal illumination this effective drift length is very short. Ordinary drift lengths ($E_0\mu\tau$) greater than a few millimeters are unusual since they can only be obtained with compensation less than 10^{13} cm^{-3} and applied biases greater than 100 V/cm. Thus for the usual experimental conditions, the effective drift length at $\omega = 0$ is shorter than a few microns and is therefore much shorter than the typical interelectrode spacing L of several hundred microns. Sweepout occurs when a restrictive boundary condition appreciably restrains the hole density in the bulk of the material. Since L_{eff} is a measure of the range of the influence of a discontinuity or boundary condition, sweepout effects would not be measurable unless L_{eff} were comparable to the interelectrode spacing L. Signal saturation with applied bias is therefore not usually observed with steady signal illumination.

Since L_D and L_{eff} are screening lengths (in the diffusion-dominated and drift-dominated case, respectively), they are very much influenced by net-charge build-up and decay processes in the material. The main effect of bipolar recombination (the use of $r = \gamma np$ rather than $r = p/\tau$) is to allow a deficit or surplus of ionized impurity states to participate in this screening process. In the high-resistivity cold-background case where $n_0 \gg p_0$, at low signal frequencies most of the screening charge is carried by the ionized impurities. Under dc conditions the carrier densities adjust themselves so that hole generation equals hole recombination. Thus for a given signal generation rate Δg at a

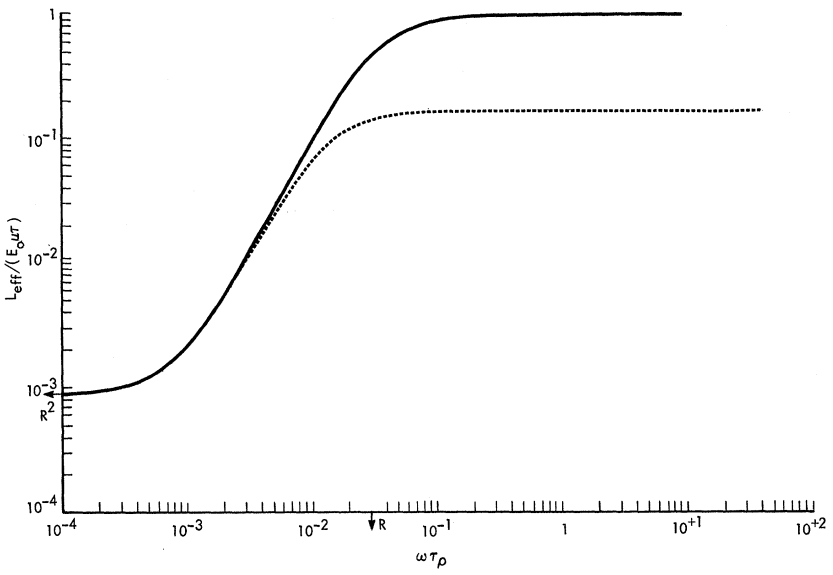

FIG. 1. Normalized plot of effective drift length vs signal modulation frequency for the case of $R = 0.03$. Solid line represents the cold-background case with $\tau_p \gg \tau$, whereas the dotted line represents one particular warm-background case where $\tau_p = 0.2\tau$.

particular point we have $\Delta n = \Delta g/\gamma p_0 - (n_0/p_0)\,\Delta p$, which can become relatively large if for some reason $\Delta p \neq \Delta g/\gamma n_0$. This process places an upper limit on the dc Debye length in high-resistivity compensated extrinsic semiconductors. However, as the signal modulation frequency increases to $\omega > (1/\tau_n)$, the ionized impurity density can no longer follow the signal, Δn near the discontinuity decreases, and L_D and L_{eff} become longer. This frequency dependence is not caused by the frequency dependence of the dielectric constant but rather by the dependence of the recombination process. The screening lengths are, of course, ultimately limited by recombination of the holes themselves (i.e., for $\omega > R(1/\tau_p)$ and $\tau_p > \tau$; $L_D \to [(e/\mu kT)(1/\tau)]^{-1/2}$ and $L_{eff} \to E_0\mu\tau$, which is the ordinary drift length).

Thus the effective drift length becomes as large as the ordinary drift length for signal modulation frequencies more than an order of magnitude lower than the inverse dielectric relaxation time. Since the ordinary drift length $(E_0\mu\tau)$ can be on the order of millimeters (larger than L), saturation of photocurrent with increasing electric field (sweepout) becomes possible. However, a restrictive boundary condition is necessary for sweepout to actually occur and the details of the process will depend on the exact solution for Δp. The constants A and B need to be determined. The value of L' as compared to the interelectrode spacing turns out to be important.

C. Case of Partial Signal Illumination

The case of uniform signal illumination is hard to understand conceptually except as an extension of the case of partial illumination. Since the solution in Eq. (7) is valid for both cases, let us therefore first consider the case of partial illumination where all of the sample is illuminated by the signal except for a small portion near the anode. In this case, the boundary between signal illumination and no signal illumination occurs not in the anode contact region, but in the bulk region where the material can be adequately characterized (see Fig. 3). In this case, there is a region of no signal where $\Delta p = 0$ (region 1 of length L_1), a transition region of length $\sim L_{eff}$ where Δp has yet to be defined (region 2), and an illuminated region in equilibrium (region 3 of length L_3) where, as expected,

$$\Delta p = \frac{\Delta g_0 (N_a - n_0)\,\tau[1 + (\tau/\tau_n)]}{[1 + (\tau/\tau_n)]^2 + \omega^2\tau^2}\cos\omega t + \frac{\Delta g_0 (N_a - n_0)\tau^2\omega \sin\omega t}{[1 + (\tau/\tau_n)]^2 + \omega^2\tau^2} \quad . \quad (17)$$

If the length of the transition region L_{eff} is much smaller than the interelectrode spacing L (low electric field case), the current in regions 1 and 3 and in the wire can be calculated by macroscopic considerations. In the small-signal case, an increase in signal illumination and conduction current in region 3 causes a negative-charge build up in the transition region. This charge builds up with the dielectric relaxation-time constant and changes the electric field and therefore the conduction current density in region 1, J_{c1}. Since the displacement current density J_{d1} in region 1 is large while the electric field is changing, it combines with the conduction current density in the small-signal case to

cancel any effect caused by the dielectric relaxation time; therefore, even though there are charge-buildup and decay processes within the sample, as long as the transition region is small, dielectric relaxation effects are invisible from the outside. In the linear case, conduction and displacement currents complement each other. See Appendix for details.

Thus in the small-signal case (relevant to the Hg-doped germanium experiments), no dielectric relaxation effects can be observed unless the length of the transition region becomes comparable to the length of the illuminated region. With high-quality semiconductor material, such as doped germanium, for large-bias electric fields this situation is possible and a satisfactory analysis then requires a microscopic analysis of the transition region using Eq. (7).

For Eq. (7) to completely describe the hole density in the illuminated region (regions 2 and 3), the constants A and B have to be determined. For an infinite sample, A must be zero in the illuminated region since physically the hole density cannot continue to increase as $x \to \infty$. For a finite sample, A need not be identically zero, but as long as $\mathrm{Re}L_1$ is small compared to L [i.e., $(kT/eE_0) \ll L$], the boundary condition at the cathode contact does not greatly perturb the hole density in the bulk of the material, and A can be set equal to zero for most purposes.

The burden of the problem is thus to determine a reasonable value for B. This is not difficult in the case of partial signal illumination. Considering $x \geq 0$ to be illuminated with signal, Δp_0 can be expressed as

$$\Delta p_0 = \frac{\Delta g_0 (N_a - n_0)\tau}{1 + \tau/\tau_n + i\omega\tau} (1 + B e^{x/L_2}) \quad \text{for } x \geq 0 \qquad (18)$$

and

$$\Delta p_0 = A e^{x/L_1} \quad \text{for } x < 0 . \qquad (19)$$

If we match Δp and $\partial \Delta p/\partial x$ at $x = 0$ (a discontinuity is impossible due to diffusion),

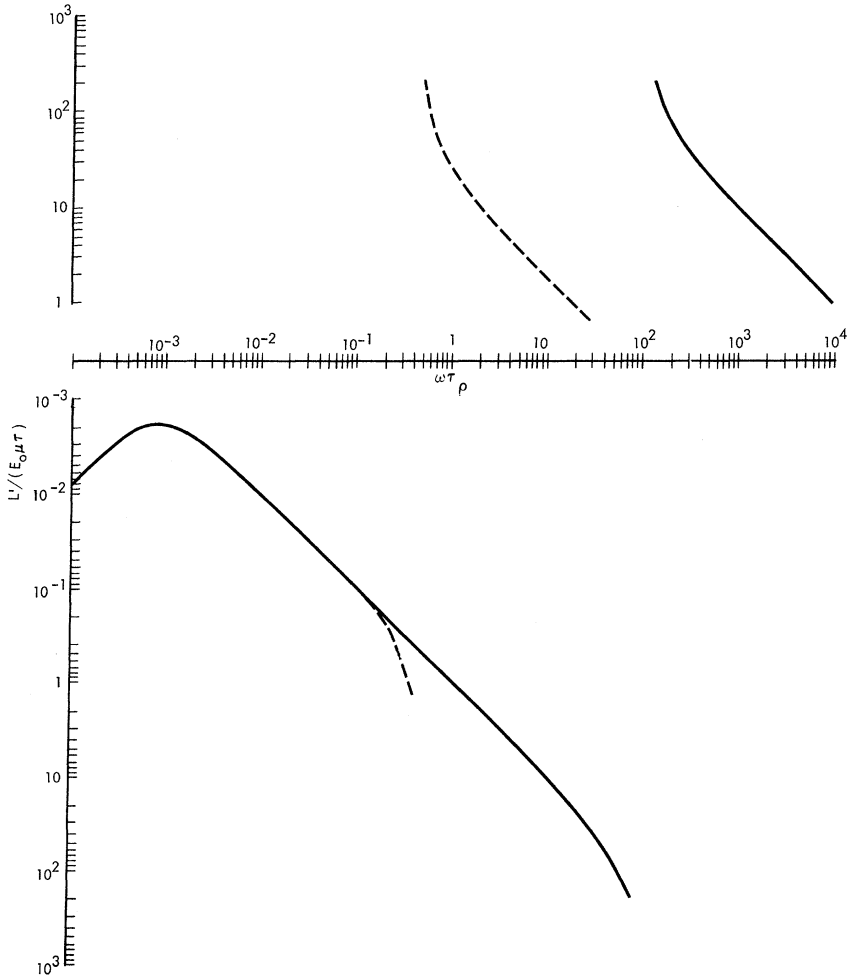

FIG. 2. Normalized plot of L' vs signal modulation frequency for the case of $R = 0.03$. Solid line represents the case where $\tau_\rho = 10^4\tau$, whereas the dotted line represents the case where $\tau_\rho = 0.2\tau$.

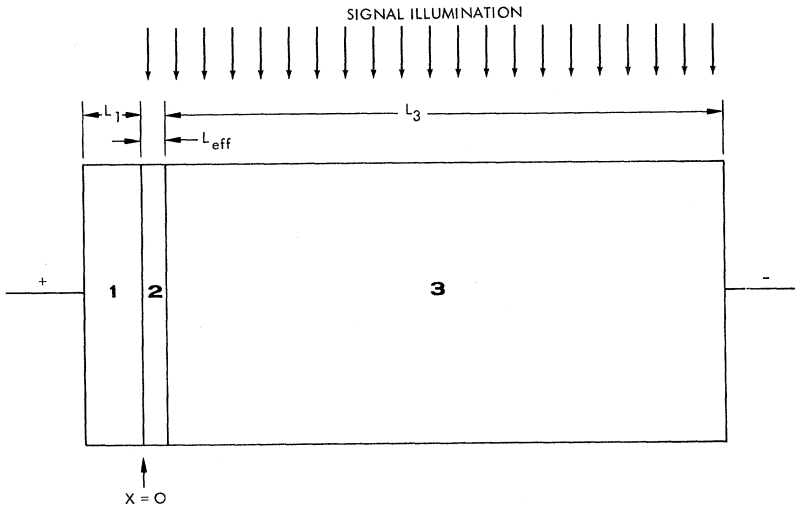

FIG. 3. Schematic of a sample partially illuminated by signal radiation.

$$B = -\left[1 + \left(\frac{1/L_{eff} + i/L'}{eE_0/kT + 1/L_{eff} + i/L'}\right)\right]^{-1}, \tag{20}$$

$$B \sim -\left[1 - i(kT/eE_0)\,(1/L')\right]. \tag{21}$$

Thus $\Delta p = 0$ corresponding to $B = -1$ is the correct boundary condition for partial signal illumination if $|L'|$ is large enough [i.e., as long as inequality (11) is satisfied and drift dominates diffusion, as is usually the case in the frequency range of most interest]. This is to be expected since holes, generated by the signal, drift away from the boundary. The hole density at a particular region is determined by the balance of generation, recombination, and drift in and drift out of that region. There are essentially two processes by which the hole density can increase from $\Delta p_0 = 0$ at the interface to the bulk equilibrium value $\Delta p_{eq} \equiv \Delta g_0(N_a - n_0)\tau/(1 + \tau/\tau_n + i\omega\tau)$. The first process involves the buildup of electrical charge in the transition region. This net charge causes a change in electric field with distance [i.e., $E \to E_0 + \Delta E$, where $\Delta E = (4\pi/\epsilon) \times \int Q'\,dx$; Q' is the charge density]. For a positive signal-generation rate, this net charge is negative and the gradient in electric field caused by this charge acts upon the equilibrium hole density p_0 to increase Δp_0. A total charge per unit area of

$$Q = -\frac{e\Delta g_0(N_a - n_0)\tau E_0 \mu \tau_\rho}{1 + \tau/\tau_n + i\omega\tau}\, e^{i\omega t} \tag{22}$$

is necessary to increase Δp_0 from zero to Δp_{eq} by this process.

The other process by which Δp_0 can increase from 0 to Δp_{eq} is by ordinary recombination, i.e., holes which are generated at $x = x'$ and drift to the right can be replaced by holes which were generated by the signal to the left of x' and which recombine at $x = x'$. Thus the length of the transition region where Δp builds up from $\Delta p_0 = 0$ at the interface to $\Delta p_0 = \Delta p_{eq}$ is limited by the ordinary drift length, i.e., by $E_0 \mu \tau$.

The high-frequency $[\omega > R(1/\tau_\rho)]$ expression for L_{eff}

$$L_{eff} = E_0\mu[(1/\tau) + (1/\tau_\rho)]^{-1} \tag{23}$$

demonstrates these two processes. For high backgrounds ($\tau_\rho < \tau$), $L_{eff} = E_0 \mu \tau_\rho$, which means that charge processes are limiting even at high frequencies and L_{eff} never becomes as long as the ordinary drift length. For low backgrounds ($\tau_\rho > \tau$), $L_{eff} = E_0 \mu \tau$ at high frequencies, so that ordinary hole recombination limits the effective drift length for this case.

We will now examine how the solution for Δp in Eq. (7) demonstrates these transport concepts. For $A = 0$ and $B = -1$, Δp_0 can be written as

$$\Delta p_0 = \frac{\Delta g_0(N_a - n_0)\tau}{1 + \tau/\tau_n + i\omega\tau}\,(1 - e^{-x/L_{eff} - ix/L'}), \tag{24}$$

which for $\omega \ll 1/\tau$, considering the real part, can be approximated as

$$\Delta p_0 = \Delta g_0 N_a \tau\{[1 - e^{-x/L_{eff}} \cos(x/L')]\cos\omega t - e^{-x/L_{eff}} \sin(x/L')\sin\omega t\}. \tag{25}$$

In the region where $L_{eff} > |L'|$, i.e., between $\omega = 1/\tau_n$ and $\omega = 1/\tau_\rho$, the solutions are very complicated with Δp_0 rising from zero and overshooting Δp_{eq}, only to fall back again, whereas the charge density Q' shows evidence of damped charge density waves with the dispersion relationship plotted in Fig. 4. See Figs. 5 and 6 for an example of the time evolution of Q' and Δp at the particular signal frequency where $L_{eff} = -10\,L'$; i.e., where $\omega = \frac{1}{10}(1/\tau_\rho)$. The solutions are very complicated. It is particularly surprising that the introduction of a restrictive boundary condition can force Δp_0 to be

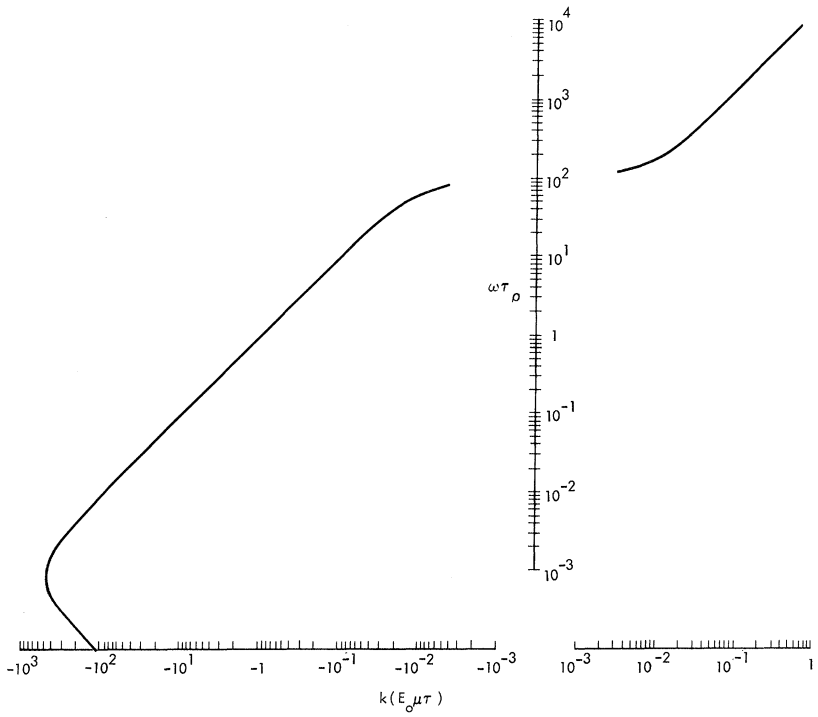

FIG. 4. Normalized dispersion relationship for space-charge density waves with $\tau_\rho = 10^4\tau$.

larger than Δp_{eq} in selected parts of the sample. Nevertheless, these solutions are physically consistent. The oscillatory wavelike structure occurs because near $x = 0$, $|\Delta n| > |\Delta p_{eq}|$ and for $\omega > 1/\tau_n$, Δn lags Δg, which means that most of the charge density is 90° out of phase with the generation rate. The length of the transition region, i.e., the decay rate of the oscillatory structure, is controlled by L_{eff}, which is limited either by the buildup of charge in phase with Δg or by hole recombination, whichever is shorter, whereas the period of the oscillatory structure (i.e., L') is controlled by the charge density out of phase with Δg. In quantitative terms,

$$\int_0^{L_{eff}} Q_1' \, dx \cong \Delta g_0 (N_a - n_0) E_0 \mu \tau \tau_\rho \tag{26}$$

as long as $L_{eff} < E_0 \mu \tau$ and

$$\int_0^{L'} Q_2' \, dx \cong \Delta g_0 (N_a - n_0) E_0 \tau \tau_\rho \, , \tag{27}$$

which is just the charge required to change Δp_0 from zero to Δp_{eq}. In the high-background case ($\tau_\rho < \tau$), hole recombination does not limit L_{eff} even for $\omega \gg R(1/\tau_\rho)$. Charge-buildup processes dominate for all frequencies and L_{eff} saturates with increasing frequency to $E_0 \mu \tau_\rho$, not $E_0 \mu \tau$.

D. Case of Uniform Signal Illumination

It is conceptually more difficult to treat the case of uniform signal illumination because the boundary between signal and no signal occurs in the contact region which is hard to characterize theoretically. The usual model of an Ohmic contact assumes a lower resistivity and a lower electric field in that region which would affect the magnitude of the local L_{eff} and L' near the contact. If the photosensitivity of the contact region is markedly poorer than that of the bulk, for whatever reason, the $\Delta p = 0$ is most likely still a good boundary condition. If the photosensitivity near the contact is not poor, then we are unable, at present, to justify this assumption. In order to proceed we will, nevertheless, assume that a correct characterization of the contact region will result in Δp being approximately zero at a position in the bulk near the contact when drift-dominated conduction prevails in the bulk, i.e., when inequality (11) holds and $|L'| \gg kT/eE_0$.

This ambiguity as to boundary condition does not occur in discussions of ambipolar sweepout (intrinsic conductivity) since, in that case, one is concerned with drift of the minority carriers and the excess majority carriers near the contact tend to make the recombination time of the minority carriers small in that region. Further, a contact which is injecting for the majority carrier is automatically blocking for the minority carrier. Thus $\Delta n_c = 0$ is a good boundary condition for p-type material where n_c is the conduction-electron density.[8] In this paper we are concerned with extrinsic photoconductivity and majority-carrier sweepout. The contact region is therefore an area of conceptual difficulty.

Lampert and Rose have developed a model for

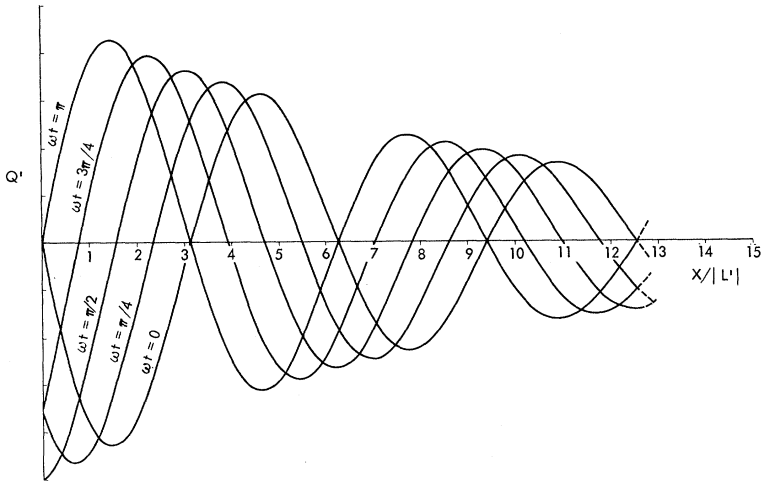

FIG. 5. Plot of charge density (in arbitrary units) vs distance from the signal illumination boundary at various times. These curves are for the signal modulation frequency where $L_{eff} = 10|L'|$.

an Ohmic contact (invisible to dc currents) and have used a macroscopic point of view to deduce a contact controlled time constant associated with a charge-buildup process for the conduction current.[9] Their calculation as it is stated in Ref. 9 cannot be correct because it leads to a time constant that is in fact nonlinear in that it depends upon relative signal strength even in the small-signal case (it becomes longer as $\Delta p/p_0 \to 0$), which is an unphysical result.

Lampert and Rose have proposed a modification of the calculation in Ref. 9 by having the swept-out negative charge concentrate initially at the cathode metal-semiconductor interface (n-type material), corresponding to an assumed initial rigidity of the contact.[10] This leads to a linear process with a contract-controlled time constant somewhat shorter than that calculated in Ref. 9. Since they do not present a complete picture of the time evolution of the contact we do not consider their argument conclusive.

E. Effective Gain

The assumption of a $\Delta p = 0$ boundary condition at the anode in the case of uniform signal illumination allows for a calculation of effective photocurrent gain defined as

$$G \equiv \overline{\Delta J_T}/\overline{\Delta g}(N_a - n_0)\, eL \,, \tag{28}$$

where $\overline{\Delta J_T}$ is the rms total photocurrent caused by the signal illumination and $\overline{\Delta g}(N_a - n_0)$ is the rms generation rate per unit length produced by the signal.

The effective gain G is a measure of the photoresponse. In the absence of sweepout, G has the usual value of $G_0 \equiv E_0 \mu \tau / L$. In the case of high-resistivity extrinsic material, $G = G_0$ for steady signal illumination; however, as we shall see, G can

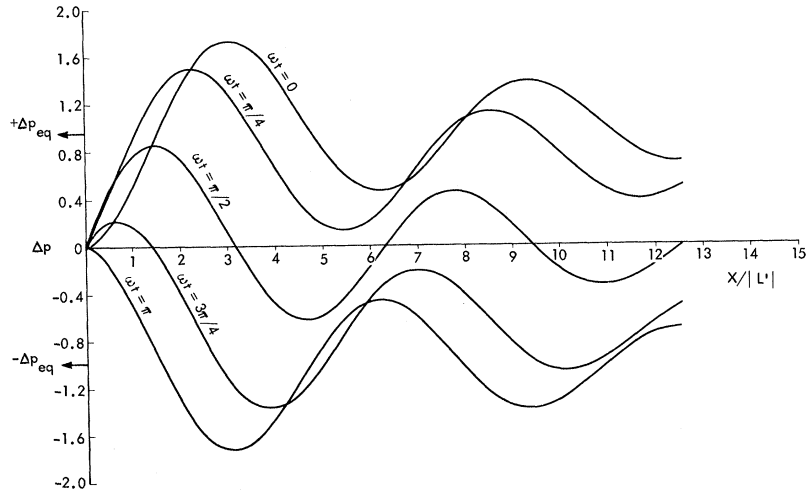

FIG. 6. Normalized plot of Δp vs distance from the signal illumination boundary at various times. These curves are for the signal modulation frequency where $L_{eff} = 10|L'|$.

decrease for higher signal modulation frequencies. A calculation of $\overline{\Delta J_T}$ including displacement current, drift current, and diffusion current for a constant applied bias in terms of the signal generation rate will allow us to calculate the effective gain G:

$$\overline{\Delta J_T} = (\Delta J_T \Delta J_T^*)^{1/2} , \tag{29}$$

$$\Delta J_T = \frac{1}{L}\int_0^L \frac{\epsilon}{4\pi}\frac{\partial \Delta E}{\partial t}\,dx + \frac{1}{L}\int_0^L e\mu p_0 \Delta E\,dx + \left(\frac{1}{L}\right)\int_0^L e\mu E_0 \Delta p\,dx + \frac{kT\mu}{L}\int_0^L \frac{\partial \Delta p}{\partial x}\,dx . \tag{30}$$

Since for a constant applied bias voltage $\int_0^L \Delta E\,dx = 0$, the first two terms can be ignored. Thus

$$\Delta J_T = \frac{e\mu E_0}{L}\int_0^L \Delta p\,dx + \frac{kT\mu}{L}\Delta p'' , \tag{31}$$

where $\Delta p''$ is Δp at $x = L$. Neglect of the last term (the diffusion term) is justified if $eE_0/kT \gg 1/L$, which is the case for the experimental conditions of interest where $E > 1$ V/cm, $L > 100$ μ, and $T < 30$ °K.

Use of the solution for Δp in Eq. (25) leads to

$$\Delta J_T = \Delta g_0 N_a \tau \mathrm{Re}\left[e\mu E_0\left(1 - \frac{L_3 + iL_4}{L}\left(1 - e^{-L/L_{\mathrm{eff}} - iL/L'}\right)\right)\frac{1}{1+i\omega\tau}\right]\cos\omega t - \Delta g_0 N_a \tau \mathrm{Im}\left[e\mu E_0\left(1 - \frac{L_3 + iL_4}{L}\left(1 - e^{-L/L_{\mathrm{eff}} - iL/L'}\right)\right)\frac{1}{1+i\omega\tau}\right]\sin\omega t , \tag{32}$$

where, for

$$1/\tau_n < \omega < 1/(\tau\tau_p) ,$$

we have

$$L_3 = \frac{E_0\mu\tau(\omega\tau_p)^2}{[1 + R^2/\omega^2\tau_p^2][1 + \omega^2\tau_p^2(1 + R^2/\omega^2\tau_p^2)^{-2}]} \tag{33}$$

and

$$L_4 = E_0\mu\tau\,\frac{\omega\tau_p}{1 + \omega^2\tau_p^2(1 + R^2/\omega^2\tau_p^2)^{-2}} . \tag{34}$$

From Eqs. (28) and (32)

$$G = G_0\left(1 - 2\frac{L_3}{L} + \frac{L_3^2 + L_4^2}{L^2} + \frac{L_3^2 + L_4^2}{L^2}e^{-2L/L_{\mathrm{eff}}} - \frac{L_3^2 + L_4^2}{L^2}\,2e^{-L/L_{\mathrm{eff}}}\cos\frac{L}{L'} + 2\frac{L_3}{L}e^{-L/L_{\mathrm{eff}}} \times \cos\frac{L}{L'} + 2\frac{L_4}{L}e^{-L/L_{\mathrm{eff}}}\sin\frac{L}{L'}\right)^{1/2}(1 + \omega^2\tau^2)^{-1/2} . \tag{35}$$

For the case of $\tau_p > \tau$, G is plotted vs ω for various values of G_0 in Fig. 7, and vs G_0 for various values of ω in Fig. 8. These figures demonstrate the sweepout effect. For $G_0 < 1/R^2$, at low frequencies the effective gain is just $G_0 = E_0\mu\tau/L$ but as the signal frequency approaches $1/\tau_p$, sweepout occurs and the effective gain is less than unity for $\omega \geq 1/\tau_p$. With $G_0 \gg 1$, G saturates to $\frac{1}{2}$ for $\omega \gg (1/\tau_p)$. If τ_p were shorter than τ (high backgrounds), the gain curves would saturate to a value of $\frac{1}{2}(\tau/\tau_p)$. As G_0 approaches $1/R^2$ ($\sim 10^3$) some sweepout degradation in G also occurs for $\omega = 0$. G at $\omega = 0$ is in fact limited to $\frac{1}{2}(1/R^2)$ for $G_0 \gg 1/R^2$.

In the calculation for G, the A was set equal to zero [corresponding very approximately to a boundary condition at the cathode of $\partial\Delta p/\partial x = 0$ for $\omega > (1/\tau_p)/G_0$]. Since L_1 is typically much smaller than L, the addition of a specific boundary condition at the cathode should make very little difference to Figs. 7 and 8. However, there may be some change in the asymptotic solutions. For instance, the imposition of a $\Delta p = 0$ boundary condition at the cathode would make $G \to 0$ as $G_0 \to \infty$ for $\omega > 1/\tau_p$. There is no physical reason to believe that $\Delta p = 0$ at the cathode is correct.

It is now appropriate to attempt to explain in an approximate manner the physical basis for gain-saturation curves in Figs. 7 and 8. Gain saturation occurs when the average value of Δp_0, i.e., $(1/L)\int_0^L \Delta p_0\,dx$, is decreased from Δp_{eq}. Significant sweepout can occur for $G_0 > 1$. For $L_{\mathrm{eff}} < L$ [i.e., $\omega < R(1/\tau_p)/G_0^{1/2}$ and $G_0 < R^{-2}$] Δp_0 throughout most of the sample is equal to Δp_{eq} and no sweepout occurs. For $\omega > R(1/\tau_p)/G_0^{1/2}$, L_{eff} is greater than L and the structure in Δp_0 caused by the boundary condition at the anode extends throughout the sample. For signal frequencies just above $R(1/\tau_p)/G_0^{1/2}$, $L' \ll L_{\mathrm{eff}}$ so that this structure is rapidly oscillating in space (see Fig. 6), and the effect on the average of Δp_0 is negligible so that sweepout has yet to degrade the effective gain. For higher signal frequencies, L' becomes comparable to L and the cancellation becomes poor. This can have either a positive or negative effect on G, depending upon whether the cathode comes at a high point or a low point in Δp. This is the cause of the irregular structure in G vs ω seen near $\omega = (1/\tau_p)/G_0$ in Fig. 7. When L' is greater than L, i.e., $\omega > (1/\tau_p)/G_0$, the net effect of the structure in Δp vs x can only be negative, real sweepout occurs, and G falls off at 3 dB/octave, eventually saturating to the value of $\frac{1}{2}$ for $\omega \gg 1/\tau_p$.

The irregular structure in G vs ω for ω just be-

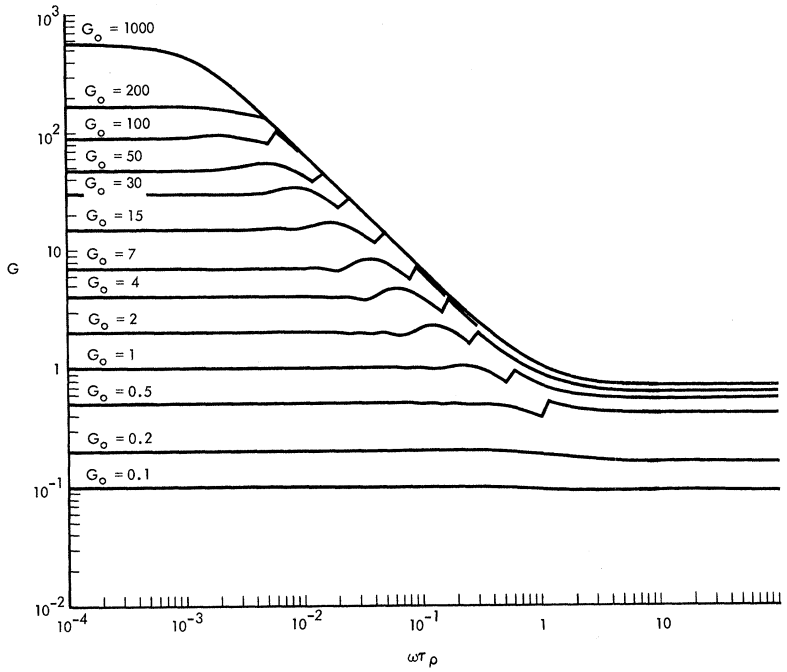

FIG. 7. Plot of photoconductive gain vs signal modulation frequency (normalized) for different values of G_0 with $\tau_\rho \gg \tau$.

low $(1/\tau_\rho)/G$, hereafter called the gain structure, depends upon the sharp structure in Δp vs x (see Fig. 6). This structure in Δp was derived for the case of drift-dominated transport, i.e., for

$$E_0 \gg \left|2kT/eL_D(\omega)\right| , \tag{36}$$

which for

$$1/\tau_n < \omega < [(1/\tau)(1/\tau_\rho)]^{1/2}, \quad \tau_\rho > \tau \tag{37}$$

can be reduced to

$$\frac{\mu\tau\omega\tau_\rho}{(1+\omega^2\tau_\rho^2)^{1/2}} \gg \frac{4kT}{eE_0^2} . \tag{38}$$

The gain structure occurs for $G_0 > 1$ with

$$\omega \sim \frac{1/\tau_\rho}{G_0} , \tag{39}$$

so that the necessary inequality for the neglect of diffusion in the important frequency region becomes

$$L \gg 4kT/eE_0 . \tag{40}$$

If diffusion were important, a much smoother Δp-vs-x curve would be expected; thus the necessary sharp structure in Δp vs x can be washed out by diffusion for small samples and small applied fields. Any inhomogeneities in τ or τ_ρ in the sample will cause the observed G-vs-ω curve to be an average of the appropriate calculated curve. This averaging would make it impossible to observe the gain structure.

Extreme caution should be exercised in attempting to find simpler approximate formulas for the gain expression in Eq. (35). However, two asymptotic approximations are useful. When $L_{\text{eff}} \gg L$ and $|L'| \gg L$, i.e., $\omega > R/(\tau_\rho G_0^{1/2})$ and $1/(\tau_\rho G_0) < \omega < G_0/\tau$ for $G_0 \gg 1$,

$$G \approx \frac{\{(\tfrac{1}{2})^2 + [\tfrac{1}{2}(L_{\text{eff}}/L')]^2\}^{1/2}}{(1+\omega^2\tau^2)^{1/2}} , \tag{41}$$

which for $R(1/\tau_\rho) < \omega < (1/\tau\tau_\rho)^{1/2}$ leads to

$$G \approx \{(\tfrac{1}{2})^2 + [\tfrac{1}{2}(1/\omega\tau_\rho)]^2\}^{1/2} , \tag{42}$$

which is independent of G_0 and saturates to $\frac{1}{2}$ for $\omega > 1/\tau_\rho$. This value of $\frac{1}{2}$ is maintained for higher modulation frequencies up to $\omega = G_0/\tau$, where lifetime effect starts to degrade the effective gain.

For $|L'| \gg L_{\text{eff}}$, i.e., $1/\tau_\rho \ll \omega \ll 1/\tau$,

$$G \approx G_0[1 - G_0(1 - e^{-1/G_0})] . \tag{43}$$

Thus for high frequencies, G is independent of ω and saturates to $\frac{1}{2}$ for large G_0. These results are, of course, dependent on the boundary conditions that were used to calculate Δp. As we have already mentioned, if a $\Delta p = 0$ boundary condition had been imposed at the cathode as well as the anode, G would go through a maximum and eventually approach zero for increasing G_0.

If $\Delta p = 0$ (making $B = -1$) were not strictly adhered to at the anode, a somewhat different behavior would ensue. Suppose $B = -1 + \delta$ where δ was real, then for $\omega > (1/\tau_\rho)/G_0$, $\omega > R(1/\tau_\rho)$, $\omega < 1/\tau$, and $G_0 \gg 1$,

$$G \approx \{[G_0\delta + \tfrac{1}{2}(1-\delta)]^2 + [\tfrac{1}{2}(1/\omega\tau_\rho)(1-\delta)]^2\}^{1/2} \tag{44}$$

and, for $\omega \gg 1/\tau_\rho$,

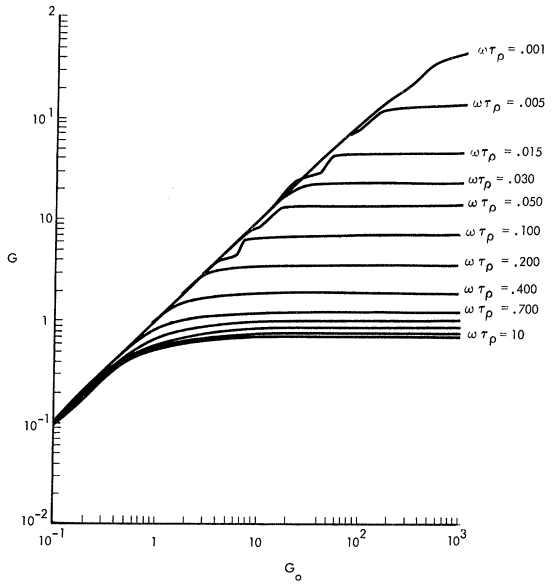

FIG. 8. Normalized plot of photoconductive gain vs G_0 for different values of signal modulation frequency.

$$G \approx G_0[1 - G_0(1-\delta)(1 - e^{-1/G_0}] , \tag{45}$$

which does not saturate to $\frac{1}{2}$ for large G_0 but rather to $\frac{1}{2} + (G_0 - \frac{1}{2})\delta$, so that for this boundary condition G can continue to increase with increasing electric field G_0, even for high signal frequencies. Complete gain saturation with increasing electric field will *not* occur unless $\Delta p = 0$ at the anode becomes the correct boundary condition. Unfortunately, if the boundary condition involved a transition region, it is conceivable that the proper value of B was frequency and/or electric field dependent.

We can use Eq. (42) to form an approximate gain-bandwidth product when $G_0 > 1$. For $G_0 < 1/R^2$, G at $\omega = 0$ is G_0 and if $G = \frac{1}{2}G_0$ at $\omega = \omega_{1/2}$, the gain-bandwidth product is

$$G_0\omega_{1/2} = 1/\tau_p . \tag{46}$$

As $G_0 \to 1/R^2$, G will be degraded from G_0 at $\omega = 0$ but the gain-bandwidth product will remain $1/\tau_p$. This result is very reminiscent of the work of Rose and Lampert who considered a somewhat different physical process (a limit on G set by space-charge injection) and derived a photoconductor gain-bandwidth-product limitation of $M(1/\tau_p)$ where M represents the ratio of stationary (trapped) to free charge.[11] The M would have to be unity in our case for the two expressions for gain-bandwidth product to agree. However, straightforward application of Rose's concepts to our situation (considering the limit on space-charge injection) would suggest that at $\omega = 0$, $M = \tau_n/\tau$ (not unity), and that M would seem to decrease for signal frequency greater than $1/\tau_n$ and drop to τ_p/τ for $\omega = 1/\tau_p$.

The introduction of sweepout limitations clearly introduces a new dimension to considerations of photoconductor gain greater than unity in extrinsic semiconductors.

For a $\Delta p = 0$ boundary condition at the anode, sweepout will limit the effective dc photoconductive gain to $\frac{1}{2}(1/R^2 + \tau/\tau_p)$ for values of G_0 greater than $1/R^2 + \tau/\tau_p$. This upper limit is the same one as would be derived by restricting G_0 to values which would avoid space-charge injection. In the case where $G_0 < (1/R^2 + \tau/\tau_p)$, sweepout will not influence the dc photoconductive gain; however, it will limit the bandwidth leading to a gain-bandwidth product of $1/\tau_p$. Sweepout will provide the limitation on gain-bandwidth product whenever

$$E_0\mu\,(1/\tau + 1/\tau_p)^{-1} > L . \tag{47}$$

Under the usual (background-limited) experimental conditions, at low operating temperatures τ_p is related to τ by

$$\tau_p = \epsilon t/4\pi J_b \tau e\mu , \tag{48}$$

so that sweepout can only be observed if

$$\frac{E_0\mu}{L} > C \equiv \frac{1}{\tau} + \frac{4\pi e\mu\tau J_b}{\epsilon t} . \tag{49}$$

Thus sweepout can only be observed with high mobilities, delicate compensation to increase τ, and cold backgrounds. See Fig. 9 for the case of Hg-doped germanium. At high effective backgrounds where τ_p is shorter than τ, the high-frequency value of L_{eff} decreases with increasing background so that sweepout effects become more and more difficult to observe.

It has just recently come to the attention of the authors that Russian workers have developed an expression similar to Eq. (35) in their analysis of contact phenomena concerning n-type gold-doped germanium.[12] Their analysis is incomplete in that they use a form for the recombination which ignores the phenomena of near-equilibrium local generation and recombination which, as we have seen, is so important to the screening of a discontinuity at low frequencies. The analysis presented here can be related to the work of Van Roosbroeck who analyzes two-carrier transports in the "relaxation case" (i.e., with $\tau_p > \tau$).[13] An analogy with two-carrier results is straightforward if extrinsic photoconductivity in Hg-doped germanium is considered to be intrinsic photoconductivity in an n-type material with zero electron mobility. In the Hg-doped germanium analog $\tau_{pn} > \tau_n > \tau_{pp} > \tau_p$ ($\tau_{pn} = \epsilon/4\pi e\mu_n n_0$, $\tau_p = 1/\gamma n_0$, etc.), whereas for the usual n-type two-carrier relaxation case with finite electron mobility, $\tau_{pp} > \tau_n > \tau_{pn} > \tau_p$. In both cases the approximation of near-equilibrium local generation and

recombination breaks down for $\omega > 1/\tau_n$. However, in the "usual" two-carrier case the screening lengths are not affected until $\omega > 1/\tau_p$, whereas for the Hg-doped germanium case the magnitude of the screening lengths changes at lower frequencies.

Sweepout in extrinsic materials is an insulator phenomenon but it can only be observed in high-quality trap-free material with low enough backgrounds. The theory we have presented, except for the restrictive boundary condition $\Delta p = 0$ at the injecting anode, is quite general in character. It should apply to germanium, silicon, and even wider band-gap materials but the inequality of Eq. (49) may not apply for most wide band-gap materials. Wide-band-gap insulators meet the requirements for high resistivity but they can have hopping mobilities and serious trapping problems. Material quality is usually not high enough to allow for long recombination times so that experimentally photoconductive gains are less than unity. Experiments with doped germanium and silicon under cold-background conditions allow insulator effects to be studied without the usual limitation of poor material quality.

III. EXPERIMENT

Photoconductive measurements were taken on a sample of Hg-doped germanium compensated with Sb which demonstrated an exceptionally large dc photoconductive gain. The sample had dimensions of 254 $\mu \times 762$ $\mu \times 5.60$ mm with contacts on the 726-$\mu \times 5.60$-mm sides. One 254×762-μ face was exposed to infrared radiation. The sample was mounted on the base of a liquid-neon Dewar. A copper enclosure essentially eliminated all radiation from warm parts of the assembly. Steady background radiation was supplied from a $Pb_{1-x}Sn_xTe$ light-emitting diode, emitting near 10 μ while ac signal radiation was supplied from an InAs diode emitting at ~2.7 μ.

In addition to the sample, a carbon composition load resistor and a transistor preamplifier were mounted on the base of the Dewar. The preamplifier was connected in the emitter follower configuration and had a gain of 0.96. The bias voltage applied to the sample V_D was measured at the output of this preamplifier so that the true voltage applied to the sample is 4% higher than V_D. The measured resistance of the load resistor varied with background and with bias voltage applied to the sample by as much as 30%. $R_L = 1.4 \times 10^8$ Ω was the most frequent value. Corrections for the variations in R_L are included in the discussion that follows. However, some difficulty was encountered in accurately measuring this resistance since di-

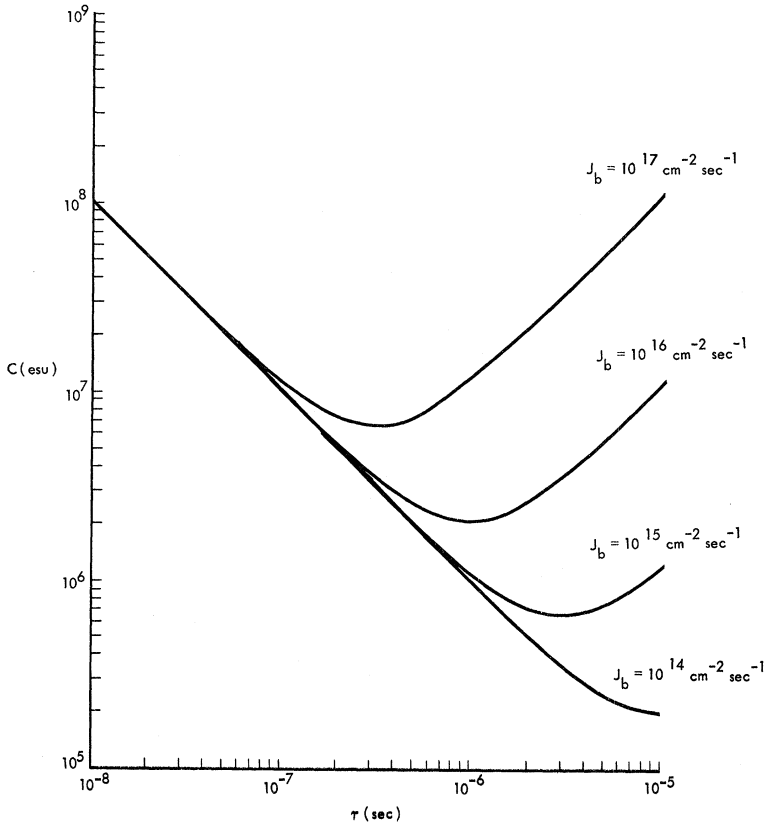

FIG. 9. Plot of $C = E_0\mu/L$ necessary to observe sweepout in Hg-doped germanium vs recombination time for different values of effective-background flux density.

rect access to the sample-load resistor interconnection was not available from outside the Dewar.

The main objective of these experiments was to gather gain-saturation information under conditions of constant sample resistance (i.e., constant τ_ρ). Signal illumination was uniformly applied to the exposed sample surface. Figure 10 shows the I-V curve of the sample at 27 °K under conditions of constant background. The voltages recorded on this curve represent the bias voltages measured at the output of the preamplifier. The maximum bias of 6 V corresponds to a bias field of 246 V/cm. The dc nonlinearity can be associated with the dependence of the $\mu\tau$ product on bias electric field which has been previously observed in Hg-doped germanium or possibly to contact-related phenomena.[14] The nonlinearity results in changes in resistance by a factor of 3 over the range of bias fields that were studied. It was felt that a change in τ_ρ by a factor of 3 would complicate the results, so that unless otherwise noted the background was adjusted so that the sample resistance R_D remained $3\times10^9\ \Omega$ for the gain-saturation measurements. The elemental capacitance of the sample was calculated to be 2.4 pF, so that this resistance would correspond to $f_\rho = 1/2\pi\tau_\rho = 22$ Hz if the resistivity were uniform throughout the sample. All measurements were taken under small-signal conditions with $\Delta R_D/R_D < \frac{1}{20}$.

The analysis leading to Eq. (35) required that the hole transport be drift dominated, i.e., that inequality (11) be satisfied. This requires that inequality (50) be satisfied.

Thus for the experimental case at hand with $\omega\tau_\rho > \frac{1}{10}$ the transport will be drift dominated for $E_0 > 2$ V/cm or for biases greater than 0.05 V which was the usual case.

Figure 10 also shows the "dc" response vs bias. This curve was obtained by measuring the response to a step function in signal illumination projected on an oscilloscope with about 2–3-sec wait for time constants to die out. This curve, which should measure G_0, tracks the I-vs-V_D curve (Fig. 10) quite well at low voltages with the same slope of 1.5. However, more saturation is evidenced for $V_D > 1.5$ V. As we shall see, this added saturation could be due to residual dielectric relaxation effects resulting from the fact that the step-function measurement is not as "dc" as the resistance measurement. If the high-bias-voltage part of the dc response is corrected to have the same slope as the R_D-vs-V_D curve, the dotted curve results and it is this corrected curve that is used to represent the truly dc situation in the calibration which follows.

During one part of the experiment the signal emitter was calibrated with reference to a chopped blackbody source after the copper enclosure had been removed (room-temperature background situation resulting in an effective background of $J_b = 5\times10^{16}$ photons/cm^2 sec). Use of an idealized spectral response curve for Hg-doped Ge material then allows for a calculation of the low-background ηG product from the measurements of low-background current responsivity (η represents the quantum efficiency of the sample). At 6-V bias, the step-function response that was actually measured corresponded to an ηG product of 4.1. Measurements of background-induced noise and responsivity with room-temperature backgrounds (background-limited conditions) indicate a quantum efficiency of ~0.18. This suggests a low-background photoconductive gain of approximately 29 at $V_D = 6$ V for the sample which we used. The sample became excessively noisy for V_D exceeding 6 V. If $\eta = 0.18$ is assumed, then the G_0-vs-V_D curve of Fig. 10 can be derived. Since the measured value of G was so much less than possible values for $1/R^2$, the possibility of sweepout or significant current injection under truly dc conditions can be ignored. The dc gain can then be associated with G_0. This leads to a maximum value for $\mu\tau$, at a bias of 2 V, of ~0.005 cm^2/V.

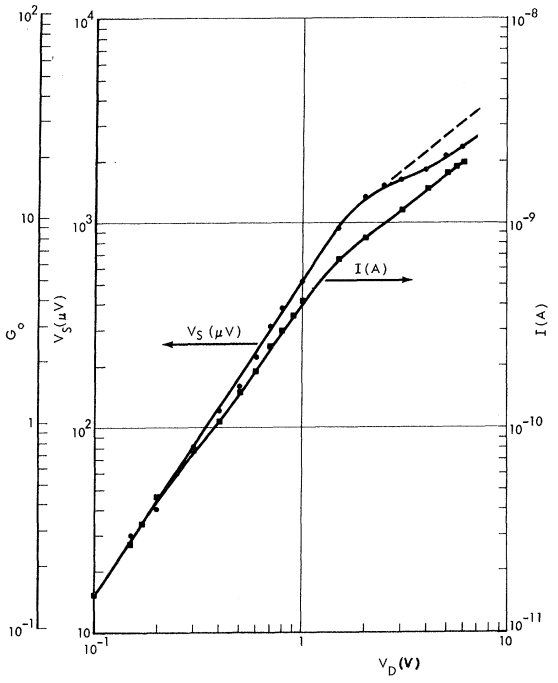

FIG. 10. Plot of observed dc current vs sample bias voltage and plot of dc response to a step function in signal illumination vs bias voltage.

The response to a modulated photosignal was measured by using a wave analyzer with a 1-cycle bandwidth. The saturation of photoresponse with increasing signal modulation frequency for various

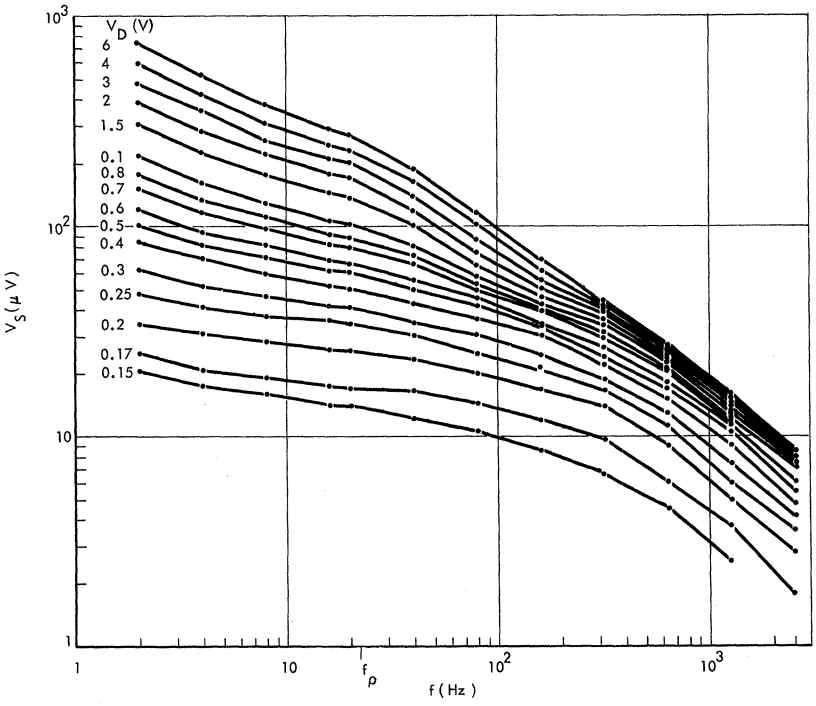

FIG. 11. Plot of observed photoconductive response vs signal modulation frequency for different bias voltages.

values of bias voltage keeping R_D fixed at 3×10^9 Ω can be observed in Fig. 11. The approximately 3-dB/octave falloff in signal for frequencies greater than 250 Hz can be attributed to an R_LC_T time constant (C_T is the *total* input capacitance at the preamplifier input node) which is not associated with any change in effective gain. The frequency dependence of the signal at lower frequencies is the gain-saturation effect. This curve should be compared with curve 7 predicted by theory. There is general agreement, but for the highest values of G_0 the slope of the curve varies between -0.5 and -0.75 and gain degradation is observed all the way from 2 to 300 Hz on both sides of $f_\rho = 22$ Hz. This is a weaker dependence than the theoretical prediction (for $\Delta p = 0$) which predicts a slope of -1 with the degradation taking place on the low-frequency side of f_ρ.

Figure 12 plots the same data in a different way and should be compared with Fig. 8 plotted from theory. The separation of the curves at low G_0 can be attributed to the R_LC_T time constant which is independent of bias. There is general agreement in that most of the gain saturation occurs for $G_0 \geq 1$ and the gain at $f = 2560$ saturates to 0.8 (subtracting out the R_LC_T effect) which compares remarkably well with the value predicted by theory, which is ~0.7 for $f \sim 100 f_\rho$ (decay to G equals exactly $\frac{1}{2}$ with increasing frequency is quite slow). The general saturation of the experimental curve is somewhat softer than that predicted by theory.

Figure 13 demonstrates several things. The two lower curves are low-bias-voltage-photosignal–vs–frequency curves for the condition of no added background illumination. These curves show the R_LC_T rolloff. The slope at 2560 Hz is not yet exactly -1; however, a reasonable extrapolation agrees with the $1/\sqrt{2}$ point to yield $f_{RC} = 250$ Hz which suggests $C_T = 4.5$ pF. The three higher curves were all taken at the same bias voltage but for different values of R_D. Although there was some experimental difficulty with the high-frequency portion of the $R_D = 1.2\times10^{-9}$ Ω curve, these curves demonstrate that a shift of R_D by a factor of 3 corresponds to a shift in the frequency scale by a factor of 3, which shows that the frequency dependence of gain saturation does indeed scale with resistance, as predicted by Eq. (35).

For $R_D = 3\times10^9$ Ω, two curves are superimposed on each other. One of the curves represents the scaled version of data taken with a signal flux 0.15 of that used normally. Since the curves fall on top of one another, it is safe to conclude that the gain-saturation effect is independent of signal flux in the small-signal region.

One of the authors (M. B.) has suggested that the gain-saturation curves might be fitted to a purely empirical formula of the form

$$G = \left(\frac{G_0 - \frac{1}{2}}{(1+\omega^2\tau_\rho^2)^{1/2}} + G_0\left[1 - G_0(1 - e^{-1/G_0})\right] \right) \times (1+\omega^2\tau_{RC}^2)^{-1/2} . \quad (50)$$

In this formula, that portion of the photocurrent gain greater than $\frac{1}{2}$ has a time constant of τ_ρ and gain falls off with a frequency slope of -1 for frequencies greater than τ_ρ. The experimental data do not fit this formula either; indeed the experimental curves could be interpreted as a behavior intermediate to that predicted by Eqs. (35) and (50). An intermediate behavior could occur if the boundary condition in the microscopic analysis presented in Sec. II were in fact frequency dependent and only became restrictive ($\Delta p \to 0$) for modulation frequencies greater than f' where $f' < f_\rho$. Saturation would then not start until $f \geq f'$. Since complete saturation at high enough frequencies is experienced, Δp at the anode must eventually become zero.

The effect of hole trapping was considered as a possible cause for the softer sweepout behavior observed in Fig. 11. A time constant controlled by trapping effects might well be electric field dependent, but it is unlikely that its appearance would depend on attaining a certain value of photoconductive gain. Williams has established the gain dependence of the slow response of interest here by observing the effect of a change in sample length.[2] Trapping can affect the effective drift length, however. A model with a trapping level solely connected to the valence band in the manner of Smith was examined.[15] As could be expected, trapping increases the effectiveness of the shielding and makes L_{eff} shorter. At low frequencies

$$\frac{1}{L_{eff}^{t(0)}} = \frac{1}{L_{eff}^{(0)}} + \frac{1}{E_0 \mu \tau} \frac{\tau_2}{\tau_1} \tag{51}$$

and, at high frequencies,

$$\frac{1}{L_{eff}^{t}} = E_0 \mu \left(\frac{1}{\tau} + \frac{1}{\tau_1} \right)^{-1} , \tag{52}$$

where τ_1 is the time necessary to trap a free hole and τ_2 is the time necessary to release a trapped hole (L_{eff}^t is L_{eff} with traps, and L'^t is L' with traps). L' is also affected, however, in the frequency range of interest; it retains its functional dependence with frequency, i.e., $|L'^t| \sim \omega$. Trapping would be expected to introduce an additional time constant into the response. However, since L'^t has the same functional dependence on frequency as L', the frequency behavior associated with sweepout should not change. Trapping therefore cannot explain the softer sweepout behavior observed in Figs. 11 and 12.

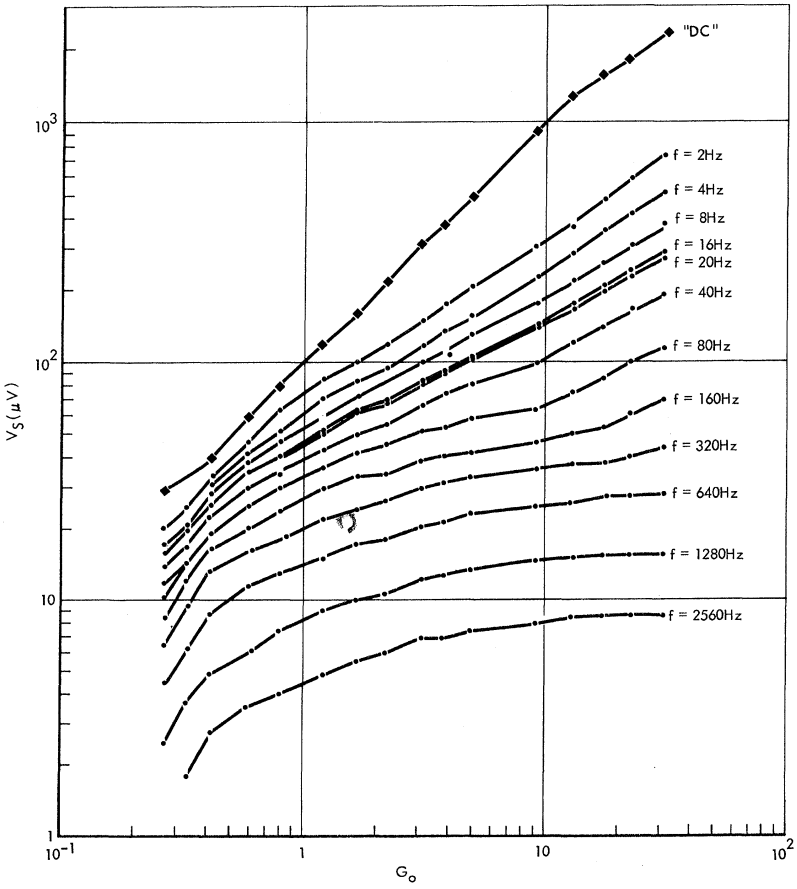

FIG. 12. Plot of observed photoconductive response vs dc photoconductive gain for different signal modulation frequencies.

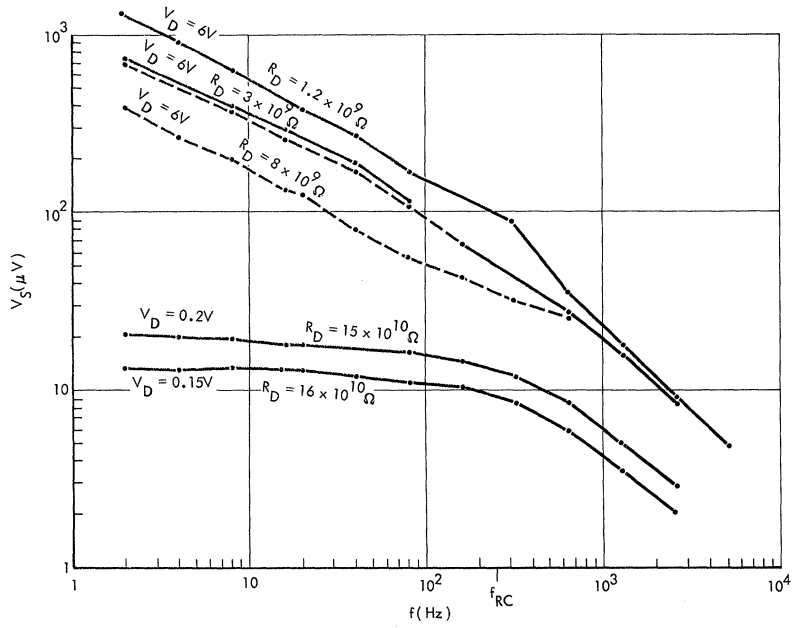

FIG. 13. Plot of observed photoconductive response vs signal modulation frequency for different sample resistances and different bias voltages. Dotted line represents normalized measurements taken with 15% of the usual signal intensity.

The lack of exact fit between theory and experiment, Figs. 7 and 11, can also be explained by considering the effect of an inhomogeneity in resistivity in the sample. Crudely, if this were the case, there would be an averaging of G-vs-G_0 and ω curves since different parts of the sample would have different values of τ_ρ. This would lead to a general softening of the effect, i.e., a slower falloff with frequency and a less abrupt saturation with increasing bias, just as was observed. An inhomogeneity in resistivity could be caused by an inhomogeneous illumination by background light (to be expected in a sample of such thick geometry) or by an inhomogeneity in the material itself caused either by an inhomogeneity in Hg doping which would vary the absorption or an inhomogeneity in compensation which would vary τ. An inhomogeneous illumination by background light cannot be the only effect since a slope of -1 was not observed for $R_D = 8 \times 10^9$-Ω curve in Fig. 13 where only thermal generation was present. An inhomogeneity in the material itself is to be expected in samples picked for maximum dc photoconductive gain since the compensation needs to be very exact and small fluctuations in the balance can change τ.

It is very difficult to analyze the effect of an inhomogeneity which occurs along a bias electric field line since the analysis of the effect of such an inhomogeneity requires that the solutions for Δp indifferent parts of the sample be matched at the interfaces. Inhomogeneities which occur perpendicular to the electric field lines can be analyzed by averaging gain values obtained for different G_0 and τ_ρ. If the inhomogeneity were caused by variations in τ or if the absorption of signal took place in the same part of the sample as the background, the tendency would be to shift the bulk of the falloff in signal to higher frequencies than that which would be predicted by using $\tau_\rho = R_D C_D$ since the signal would come mostly from regions of low resistivity. A shift of about a factor of 5 would be consistent with the data observed.

An inhomogeneity could occur in a bewilderingly large number of ways so that an attempt to exactly fit the data without some knowledge of the distribution of the inhomogeneity is doomed to failure. Nevertheless, some indication of the effect of inhomogeneities can be obtained by considering an average gain of the form

$$\langle G \rangle = \frac{1}{N+1} \sum_{n=0}^{N} G(G_0, \omega, 2^n \tau_\rho') \,, \qquad \langle \tau_\rho \rangle = 2^{N/2} \tau_\rho' \,. \tag{53}$$

This is an average of different parts of a sample which had different τ_ρ values and roughly represents the measured gain of an inhomogeneous sample. $N \approx 5$ was required to produce a slope of -0.75 for the $G_0 \sim 32$ curve. Figures 14 and 15 show Eq. (52) for $N = 5$. The curves in Figs. 14 and 15 show a strong resemblance to the experimental data which suggests that inhomogeneities in resistivity ρ with a standard deviation of about 10 $\langle \rho \rangle$ would account for the softening of the curves that was observed.

Incomplete data taken with larger samples of considerably lower maximum photoconductive gain have shown signal falloff slopes of ~ 0.8, and the curves in Ref. 12, taken with n-type gold-doped Ge, show a falloff slope of -1. The necessary sample geometry for high quantum efficiency and

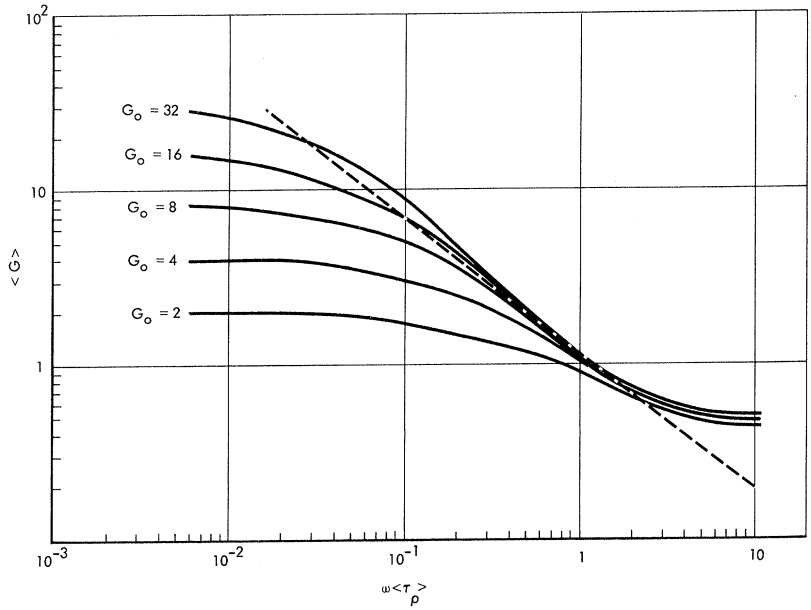

FIG. 14. Plot of the photoconductive gain of an inhomogeneous sample vs signal modulation frequency for different values of G_0.

high gain are a severe constraint on the experiment. The light pipe configuration makes measurements with a nonuniform signal illumination very difficult so that we are burdened with the uncertainty in boundary condition caused by uniform signal illumination.

IV. CONCLUSIONS

The consequences of the frequency dependence of the Debye length on photocarrier transport in compensated extrinsic photoconductors have been considered in detail. For the case of uniform

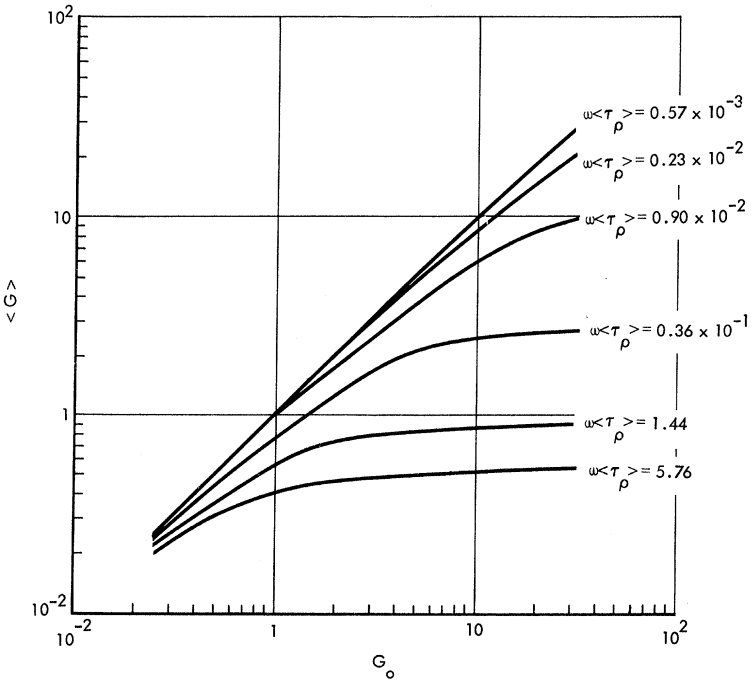

FIG. 15. Plot of the photoconductive gain of an inhomogeneous sample vs G_0 for different signal modulation frequencies.

signal illumination, gain-saturation curves have been derived using the boundary condition of $\Delta p = 0$ at the anode. This led to a gain bandwidth product of $1/\tau_\rho$ caused by majority-carrier sweepout. The prediction of the theory has been compared with a sample of Hg-doped germanium which provided a dc photoconductive gain of ~30. There was general agreement with theory but the experimental curves showed a somewhat softer behavior than that predicted theoretically. This lack of agreement could be explained if the sample resistivity were inhomogeneous.

ACKNOWLEDGMENTS

The authors would like to acknowledge contributions made by R. L. Williams whose original experiments in this area inspired this investigation. Conversations with J. Blakemore, A. Rose, M. Lampert, R. B. Emmons, and C. Jeffus have also been helpful. M. Tipps assisted with the experiments. E. Williams helped with the computer calculations.

APPENDIX

If the length of the transition region L_{eff} is much smaller than the interelectrode spacing L (low-bias electric field case), the current in regions 1 and 3 of Fig. 3 and in the wire can be calculated from macroscopic considerations. For the case of sinusoidal signal illumination and constant voltage V across the sample, the equations which describe the charge-buildup process are

$$(\epsilon/4\pi)(\dot{E}_1 - \dot{E}_3) = J_{c3} - J_{c1} , \tag{A1}$$

$$E_3 L_3 + E_1 L_1 = V , \tag{A2}$$

$$E_3 = E_0 + \Delta E_3, \quad E_1 = E_0 + \Delta E_1,$$

$$E_0 = V/(L_1 + L_3) , \tag{A3}$$

$$\Delta\dot{E}_1 = \frac{1}{\tau_\rho}\left[\left(\frac{\Delta p_3}{p_0(1+y)}\right) E_0 - \left(1 + \frac{\Delta p_3}{p_0}\,\frac{y}{1+y}\right)\Delta E_1\right],$$

$$y = \frac{L_1}{L_3} \tag{A4}$$

for $e^{i\omega t}$ time variations of ΔE and Δp, neglecting nonlinear terms:

$$\Delta J_{d1} = \frac{\epsilon}{4\pi}\,\Delta\dot{E}_1 = \left(\frac{i\omega\tau_\rho e\mu\Delta p_3 E_0}{(1+y)(1+i\omega\tau_\rho)}\right) e^{i\omega t} , \tag{A5}$$

$$\Delta J_{c1} = e p_0 \mu \Delta E_1 = \left(\frac{e\mu\Delta p_3 E_0}{(1+y)(1+i\omega\tau_\rho)}\right) e^{i\omega t} , \tag{A6}$$

$$\Delta J_{tot} = \Delta J_{d1} + \Delta J_{c1} = \left(\frac{e\mu\Delta p_3 E_0}{1+y}\right) e^{i\omega t} = \Delta J_{c3} . \tag{A7}$$

Thus ΔJ_{tot} does not show dielectric relaxation processes.

The charge per unit area in the transition region is

$$Q = \int (\Delta J_{c1} - \Delta J_{c3})\, dt = \left(\frac{-\Delta p_3 e\mu E_0 \tau_\rho}{(1+y)(1+i\omega\tau_\rho)}\right) e^{i\omega t} . \tag{A8}$$

Any nonlinearity will destroy the complementarity of conduction and displacement current. This will make charge-buildup processes visible. If Δp is not smaller than p_0, nonlinear effects can occur and quasidielectric relaxation effects can be observed from the wire. An overshoot in photosignal which has been observed in high-resistivity alkali-halide crystals (photocurrent gain $\ll 1$) has been attributed to these nonlinear processes.[16]

The microscopic consideration involved in the solution for Δp in Eq. (7) shows the same processes taking place. For $A = 0$, $B = -1$, Q' (the net charge density) can be written in the small case for $x > 0$ without approximation as

$$Q' = \Delta Q_0' e^{i\omega t} , \tag{A9}$$

where

$$\Delta Q_0' = e(\Delta p_0 - \Delta n_0)$$

$$= -e\,\frac{\Delta g_0 (N_a - n_0)\tau_n}{1 + i\omega\tau_n}\, e^{-x/L_{eff} - ix/L'} = Q_1' + iQ_2' , \tag{A10}$$

and $x = 0$ defines the boundary of signal illumination. $-Q_1$ oscillates in phase with Δg, whereas $-Q_2'$ oscillates 90° out of phase with Δg.

For the semi-infinite sample ($L \gg L_{eff}$), the total rms charge in the transition region for $1/\tau_n < \omega < 1/\tau$ is

$$\overline{Q} = (\tfrac{1}{2} Q Q^*)^{1/2} = \frac{e\Delta g_0 (N_a - n_0)(E_0\mu\tau)\tau_\rho}{[1 + \omega^2\tau_\rho^2(1 + R^2/\omega^2\tau_\rho^2)^{-1}]^{1/2}} , \tag{A11}$$

where

$$Q = \int_0^\infty Q'\, dx , \tag{A12}$$

which is approximately what was derived from macroscopic considerations in Eq. (A8).

---

*Work supported in part by the Advanced Research Projects Agency.

[1] R. L. Williams, J. Appl. Phys. 38, 4802 (1967).

[2] R. L. Williams, J. Appl. Phys. 40, 184 (1969).

[3] S. M. Ryvkin, *Photoelectric Effects in Semiconductors* (Consultants Bureau, New York, 1964), Chap. XII, p. 246.

[4] The ordinary drift length is the drift length of an individual hole; the effective drift length is a collective phenomenon.

[5] A. F. Milton, Appl. Phys. Letters 16, 285 (1970).

[6] V. A. Besfamil'naya and V. V. Ostroborodova, Fiz. Tekh. Poluprov. 3, 21 (1969) [Sov. Phys. Semicond. 3, 15 (1969)].

[7] G. Picus, J. Phys. Chem. Solids 23, 1753 (1962).

[8] E. S. Rittner, *Photoconductivity Conference*, edited by R. G. Breckenridge, B. R. Russell, and E. E. Hahn

(Wiley, New York, 1956), p. 215.
[9]M. A. Lampert and A. Rose, Phys. Rev. 113, 1236 (1959).
[10]M. A. Lampert (private communication).
[11]A. Rose and M. A. Lampert, Phys. Rev. 113, 1227 (1959).
[12]S. A. Kaufman, N. Sh. Khaikin, and G. T. Yakovleva, Fiz. Tekh. Poluprov. 3, 571 (1969) [Sov. Phys. Semicond. 3, 485 (1969)].
[13]W. Van Roosbroeck, Phys. Rev. 123, 474 (1961).
[14]M. Loewenstein and A. Honig, Phys. Rev. 144, 781 (1966).
[15]R. A. Smith, *Semiconductors* (Cambridge U. P., Cambridge, England, 1961), p. 256.
[16]M. Y. Ben Sira, B. Pratt, E. Harnik, and A. Many, Phys. Rev. 115, 554 (1959).

PHYSICAL REVIEW B VOLUME 3, NUMBER 12 15 JUNE 1971

Theory of Raman Scattering in Solids

Jan Smit
Departments of Electrical Engineering and Materials Science, University of Southern California, Los Angeles, California 90007
(Received 21 July 1970)

The Raman effect due to phonons, Landau levels, and Stark ladder levels is analyzed theoretically. For the phonons, three mechanisms are identified, and their orders of magnitude are estimated for both $\Delta n = 1$ and 2. The ratio of the intensities can be of order unity, especially when the crystal has only one narrow band gap. The resonance Raman effect is particularly strong in the band. For the electronic Raman effect from Landau levels, three similar mechanisms can be distinguished. The $\Delta n = 1$ transition can occur only in crystals without a center of symmetry, and has a strength comparable to the $\Delta n = 2$ process. It can also occur in case of broken symmetry, as in n-type Si. The Raman effect from a Stark ladder should in principle give the Fourier components of the E-k curve. Finally, it is shown that effective-mass theory for donor levels is reliable only for materials with $\epsilon > 5$, irrespective of m^*.

I. INTRODUCTION

The Raman effect in solids has been the subject of much experimental and theoretical research in recent years.[1] The theoretical approach has been generally rather phenomenological, and it is felt that as a result several characteristic features of Raman scattering in solids have not received an adequate explanation. For example, the ratio of the intensities of the $\Delta n = 2$ and $\Delta n = 1$ lines is often surprisingly large, even off-resonance. Furthermore, existing theories have difficulty explaining the large Raman cross section when the laser energy enters the continuum of excited states. Raman scattering from conduction electrons in a magnetic field (Landau levels) has been detected for $\Delta n = 1$, 2, but published theories only account for the $\Delta n = 2$ process. The role of inversion symmetry has not been elucidated.

We shall consider these points below and be more specific about the effective-interaction Hamiltonian, which is shown to arise from three mechanisms. A complete theory would become very involved, and therefore only the leading matrix elements will be shown; complete calculations can easily be made for each individual case. In addition to the inelastic light scattering from Landau levels, the possibility of a Raman effect from conduction electrons in a strong static electric field is also analyzed. In order for the band index to be a good quantum number, in both cases the fields cannot be too strong. Such a limit also exists for the validity of effective-mass theory for donor levels and is shown to imply that the dielectric constant ϵ must be substantially larger than 5, independent of the magnitude of the effective mass.

II. PHONON SCATTERING

The interaction Hamiltonian of em radiation with matter will be taken of the form

$$H_r = H_L + H_R = (e/mc)(\vec{A}_L \cdot \vec{p} + \vec{A}_R \cdot \vec{p}) , \qquad (1)$$

where $\vec{p}$ is the momentum of the electron under consideration and $\vec{A}_L$ and $\vec{A}_R$ are the vector potentials of the incident (laser) and Raman light beams, respectively. These vector potentials can be expressed in terms of creation and annihilation operators of photons according to

$$A_L = c(h/\omega\epsilon V)^{1/2}(a_L^\dagger + a_L)$$

in the dipole approximation. In first approximation, the wave function is a product of electronic, phonon, and photon wave functions. The p operator in (1) gives matrix elements between the total electronic ground state $|g\rangle$ and the excited states $|e\rangle$, but it does not change the phonon quantum number. The phonons enter into the problem in three ways. Process (a)—the equilibrium positions of the ions in $|e\rangle$ are shifted with respect to those in $|g\rangle$. Process (b)—the elastic properties of the lattice